Preis and Biedenbach *Energy Informatics* 2023, **6**(Suppl 1):33
https://doi.org/10.1186/s42162-023-00288-x

Energy Informatics

RESEARCH

Open Access

Assessing the incorporation of battery degradation in vehicle-to-grid optimization models

Valentin Preis[1*] and Florian Biedenbach[1]

From The 12th DACH+ Conference on Energy Informatics 2023
Vienna, Austria. 4-6 October 2023. https://www.energy-informatics2023.org/

*Correspondence:
vpreis@ffe.de

[1] Forschungsstelle für Energiewirtschaft e.V., Am Blütenanger 71, Munich 80995, Germany

Abstract

Bidirectional charging allows energy from the electric vehicles (EV) to be fed back into the grid, offering the possibility of price-optimized charging. However, such strategies cause higher charging cycles, which affect the cyclic aging of the battery and reduce its service life, resulting in additional costs for the user. Various approaches are used to account for battery degradation in optimizations models of bidirectional charging use-cases. In this paper, a systematic literature review is carried out to identify existing battery degradation models and to determine the most suitable one. In the models under review, degradation is integrated into the optimization's objective function. The review shows that there are mainly two strategies suitable for vehicle-to-grid (V2G) optimization problems: A weighted Ah-throughput model (wAh-model) with a constant degradation cost factor and a performance based model (pb-model) linking the degradation to measurable parameters such as capacity loss. Both models were implemented and analyzed. The results show that the wAh-model is the better optimization option, as in the pb-model the current state of health of the battery has an excessively large impact on the calculated degradation cost. It leads to excess costs due to a higher aging rate at the beginning of life which proves to be not ideal in the optimization. The sensitivity analysis reveals that altering the initial State of Health (SoH) from 95 % in the base scenario to 100 % leads to an increase in average degradation costs by factor 9.71 in the pb-model. From the evaluated base scenario the average degradation costs for the pb-model are 0.45 cent/kWh and for the wAh-model 0.23 cent/kWh.

Keywords: Cyclic aging, Battery degradation, Linear optimization, Vehicle-to-grid, Bidirectional charging, Electric vehicle, Electromobility

Introduction

A survey by the German Association of Energy and Water Industries (BDEW) reveals that acquisition costs are still a primary barrier to the adoption of EVs (Bantle and Metz 2019). However, with the ongoing development of battery and charging technology, new opportunities are emerging to steadily reduce the operating costs of EVs. By enabling the electricity stored by vehicle to be fed back into the grid, bidirectional charging represents one such possibility. The ability to charge vehicles in times of low electricity prices and discharge them during times of high electricity prices not only allows vehicle owners to generate revenue but also contributes to a more flexible energy system with regard to ancillary services (Hinterstocker et al. 2019). This opportunity is also referred to as V2G. However, these use-cases can increase the number of charge cycles in EVs. This affects the cyclic aging of the battery and shortens its service life, which is associated with additional costs. Therefore, battery aging is an elementary component in the economic analysis of bidirectional charging strategies. By implementing existing models to account for battery degradation in the FfE e.V. electric Flexibility Assessment Modelling Environment (eFlame), this paper deepens the insight into battery degradation in optimization problems and provides two strategies to include battery aging when modelling bidirectional charging strategies for EVs (Kern et al. 2023). Within the scope of this paper, the following research questions are to be answered:

- What models have been published to integrate battery degradation in market optimization problems suitable for V2G applications?
- How can the methods of published models be adapted and implemented in an existing optimization model? This inclusion of existing nonlinear battery aging models into a previously separate linear optimization model represents the main innovation presented in this paper.
- What is the impact of battery aging on bidirectional charging strategies?

This Paper is outlined as follows: Based on the results of the literature review presented later in the Introduction, suitable models are developed and implemented in the Simulation environment eFlame. This is described in the section Methodology. In the same section, a scenario is defined and the necessary data inputs for the following simulations are provided. The outcomes of these simulations, including a sensitivity analysis, are presented in Results. The results serve as a basis to identify the most appropriate model for including battery degradation into the optimization problem. In the end, a Conclusion is presented.

Based upon a review of current literature, it can be concluded that types battery aging models can largely be divided into two groups: Physio-chemical models and system level models. Naumann et al. (2020) (cf. Fig. 1) Physio-chemical models attempt to provide an internally focused understanding of battery aging. In most cases they offer a highly detailed depiction of the internal processes of a battery, and are mainly used to optimize the physical design of the battery cell. They usually combine design parameters with macro- or microscopic information of the cell. These models are much more computationally intensive and therefore hardly usable for linear optimization problems. Therefore, this Paper does not take this type of model for the degradation assessment into account. Physio-chemical models can be further subdivided into equivalent circuit models, electrochemical models, and microstructural models. Equivalent circuit models evaluate battery degradation by including components such as voltage sources, capacitors, resistors and inductors in the model (cf. Liaw et al. (2005); Erdinc et al. (2009)).

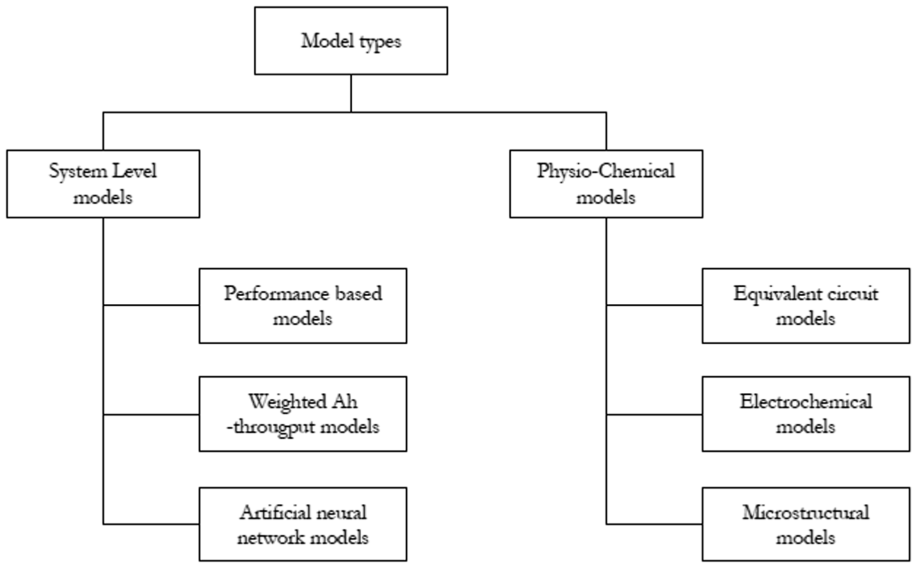

Fig. 1 Types of battery aging models

In electrochemical models the course of degradation is usually determined by numerically solving a system of nonlinear partial and algebraic equations describing the internal processes. In this model type, knowledge is gained about both electrical and chemical parameters, such as electrolyte concentrations or diffusion coefficients (cf. Prada et al. (2013); Ekström and Lindbergh (2015)). With the help of the finite element method, microstructural models reconstruct the microstructure of the electrodes and spatially solve a system of partial differential equations. Although this model type requires the greatest effort in implementation, it can also provide the most accurate results (cf. Bolay et al. (2022)). System level models consider the complete battery system from an external perspective, and determine its service life with the help of measurable operating conditions. Internal reactions or interactions are usually not considered. This type of model is usually based on empirical data sets collected in large test series. In pb-models the degradation is calculated by the change in battery parameters such as capacity loss or resistance increase. For the influencing stress factors, the course of the measured parameters is usually described by mathematical functions determined by fitting procedures (empirical models). Models which implement further theoretical considerations about the aging of the battery are referred to as semi-empirical models. (Farzin et al. 2016) The End of Life (EOL) of the battery is determined by a certain threshold value of the chosen parameter (cf. Wang et al. (2011); Swierczynski et al. (2015); Schmalstieg et al. (2014)). Studies using wAh-models connect the end of life of the battery to parameters such as charge quantity throughput or number of cycles (cf. Zhou et al. (2020); Seydenschwanz et al. (2019); Soleimani et al. (2021)). This is based on the assumption that a battery can undergo a maximal charge quantity throughput until its end of life is reached. Artificial Neural Network models (ANN-model) represent a more recent development. By using the black box approach, degradation values at the output are generated via specifications of stress factors at the input. The relationship between input and output variables can be realized by supervised or unsupervised learning. (cf. Shen et al. (2005); Johnson (2002))

However, ANN-models are not further considered in this work, because they require large data sets. Therefore, this paper concentrates on the wAh-model and the pb-model in the exploration of the presented research questions. For further analysis both types of models are implemented into eFlame through an objective based approach for further analysis. In this approach the impact of battery degradation is directly integrated as a decision variable in the objective function of the optimization problem. In addition, a constraint-based approach is also applied, which is often used to extend the lifetime of the battery. This is realized by externally restricting the operation of the battery, for example by limiting the maximum Depth of Discharge (DoD) or the number of full equivalent cycles (FEC) available per day. (Zhou et al. 2011) Regarding the type of degradation, the model considers cyclic aging of the battery, as the literature review reveals that this is the primary form of aging considered in other economic optimization (cf. Brinkel et al. (2020); Seydenschwanz et al. (2019); Soleimani et al. (2021); Schimpe et al. (2018)). Cycle life represents the maximum number of charge or discharge cycles possible for the battery, and is therefore directly dependent on the charging strategy. Calendar aging is often regarded as a non-operational factor, since in this type of aging time is the primary factor. However, in the reality the two aging phenomena occur simultaneously and separation proves to be difficult.

Methodology

Simulation environment

Both degradation models are integrated into the linear optimization model eFlame which is described in detail in Kern et al. (2022). eFlame was mainly developed to optimize the operation of bidirectional charging use-cases. Examples can be found in Kern et al. (2020, 2022), where arbitrage-trading and self-consumption optimization use-cases are analyzed. A peak-shaving use-case is published in Kern and Bukari (2021). Figure 2 shows all power flows relevant for the optimization. The optimization only considers the period in which the EVs are connected to the charging station. A non-negativity constraint applies for all decision variables. The core objective function of the linear optimization is a maximization problem. The goal of the optimization is to maximize the profit based on occurring costs and revenues. The core objective function is defined in Eq. (1).

$$max\left(\sum_{t\in T} p_{to-grid,t}\, P_{to-grid,t}\ \Delta t - p_{from-grid,t}\, P_{from-grid,t}\ \Delta t\right) \tag{1}$$

The index t represents the time steps. Revenues can be generated via the power fed into the grid $P_{to-grid,t}$ at the grid connection point (GCP). $P_{from-grid,t}$ describes the power purchased from the grid. In this paper, EVs are assumed to be the only components located at the GCP. Depending on the defined simulation scenario, different price time series $P_{to-grid,t}$ and $P_{from-grid,t}$ in €/kWh are considered. To preserve the physical consistency of the system, constraints have to be defined in the linear optimizations. For the implementation of the battery aging model, the main constraints concern the GCP and

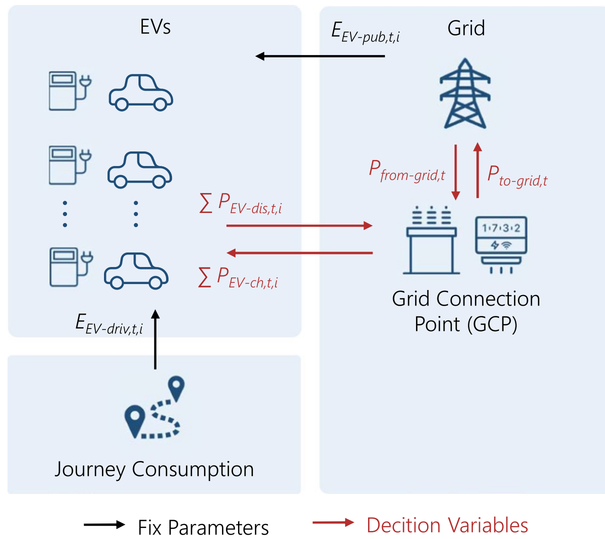

Fig. 2 Schematic representation of the optimization model

the vehicles. When considering the number of EVs N_{EV}, with respect to the physical law of energy conservation at the GCP, the power balance results in Eq. (2).

$$P_{from-grid,t} - P_{to-grid,t} = \sum_{i=1}^{N_{EV}} P_{EV-ch,t,i} - \sum_{i=1}^{N_{EV}} P_{EV-dis,t,i} \tag{2}$$

$P_{EV-ch,t,i}$ and $P_{EV-dis,t,i}$ describe the power levels with which the i-th EV is charged and discharged, respectively. This ensures that in each time step t the input power is equal to the output power. The power at the grid connection point is limited by Eqs. (3) and (4).

$$0 \leq \; P_{from-grid,t} \leq P_{GCP-max,t} \tag{3}$$

$$0 \leq \; P_{to-grid,t} \leq P_{GCP-max,t} \tag{4}$$

The parameter $P_{GCP-max,t}$ represents the maximum grid connection power. To preserve the physical consistency of the EVs, the energy balance of the vehicle battery must be maintained. With the $SoC_{EV,t,i}$ at $t = 1$, the constraint in Eq. (5) holds for the energy capacity of the battery in the first optimization step.

$$\begin{aligned} E_{EV-stored,t=1,i} =& SoC_{EV,t=1,i} \, E_{EV-cap,i} + P_{EV-ch,t,i} \, \eta_{ch} \, \Delta t \\ & - \frac{1}{\eta_{dis}} \, P_{EV-dis,t,i} \, \Delta t - E_{EV-driv,t,i} + E_{EV-pub,t,i} \end{aligned} \tag{5}$$

$E_{EV-cap,i}$ stands for the energy capacity of the i-th EV in kWh. Energy consumption of the EV while driving is expressed via $E_{EV-drive,t,i}$ and public charging is taken into account through $E_{EV-pub,t,i}$. For all further optimization steps, the energy capacity of the vehicle is calculated in Eq. (6) by the sum of all energy flows and the energy capacity $E_{EV-stored,t,i}$ from the previous time step.

$$E_{EV-stored,t,i} = E_{EV-stored,t-1,i} + P_{EV-ch,t,i}\,\eta_{ch}\,\Delta t - \frac{1}{\eta_{dis}}\,P_{EV-dis,t,i}\,\Delta t - E_{EV-driv,t,i} + E_{EV-pub,t,i} \tag{6}$$

In eFlame the energy consumption from driving is calculated by a consumption model considering the average velocity and the outdoor temperature from predefined driving profiles. The model was created with help of measured power consumptions of EVs derived from Huss et al. (2013) and Geringer and Tober (2012) and published in the projects (Pellinger and Schmid, MOS 2030) and (Samweber et al. MONA 2030). It is assumed that the remaining energy demand of $E_{EV-drive,t,i}$ for longer trips exceeding the available capacity is fulfilled by public charging. Equation (7) ensures that at no time the defined energy capacity of the battery $E_{EV-cap,i}$ is exceeded.

$$0 \le E_{EV-stored,t,i} \le E_{EV-cap,i} \tag{7}$$

The limitation of the wallbox through the maximum charging power $P_{EV-max\ ch,t,i}$ or discharging power $P_{EV-max\ dis,t,i}$ is derived from the constraints in the Eqs. (8) and (9). $Con_{EV,t,i}$ is a binary indication variable and specifies the time steps in which the vehicle is connected to the wallbox.

$$P_{EV-max\ ch,t,i}\,Con_{EV,t,i} \ge P_{EV-ch,t,i} \tag{8}$$

$$P_{EV-max\ dis,t,i}\,Con_{EV,t,i} \ge P_{EV-dis,t,i} \tag{9}$$

Further constraints concern the $SoC_{EV,t,i}$ of the EVs under consideration. In the optimization, a minimum $SoC_{EV-min\ con}$ must always be maintained when the EV is connected to the wallbox. This constraint is defined in Eq. (10).

$$E_{EV-stored,t,i} + E_{EV-buffer,t,i} \ge SoC_{EV-min\ con}\,E_{EV-cap,i}\,Con_{EV,t,i} \tag{10}$$

With the inequality in Eq. (11), the compulsory minimum $SoC_{EV-min\ dep}$ at the time of departure is given.

$$E_{EV-stored,t,i} + E_{EV-buffer,t,i} \ge SoC_{EV-min\ dep}\,E_{EV,cap,i}\,Dep_{EV,t,i} \tag{11}$$

In both equations, $E_{EV-buffer,t,i}$ is implemented to guarantee adherence to the State of Charge (SoC) constraints. Thus, for example, $SoC_{EV-min\ dep}$ is also ensured for the case when long trips follow each other in small intervals and the obliged SoC could no longer be adhered even with maximum charging power. $E_{EV-buffer,t,i}$ therefore acts as an auxiliary variable if the constraints cannot be met.

Cyclic aging model

Both models for degradation assessment build on the previously developed cyclic aging model described in Naumann et al. (2020). The model was chosen based on prevailing requirements. Regarding the Simulation environment, the model must be code-based, implementable in MATLAB and integrable in a linear optimization problem. To ensure applicability of the results, the cyclic degradation model should be based on a suitable cell for V2G applications evaluated with a large test matrix. Table 1 shows the cell used in the study. Other considered aspects are the analyzed stress factors and the additional computing time, since simulations of market optimization problems often take place over a longer period of time with high resolution.

In Naumann et al. (2020) cyclic aging is examined with regard to both the decrease in available capacity and the increase in internal resistance of the cell. The results from the study reveal that due to the cyclic stress on the cell, the decrease in available capacity is higher than the increase in internal resistance. Thus, both models assessed here use the evolution of available capacity to calculate aging. Based on the test series, the cyclic aging model is developed from the measured experimental data using curve fitting. The experimental series to evaluate degradation is comprised of 19 test points with different combinations of temperature, $C - Rate$, DoD and SoC. The basic fitting function describing the decrease in available capacity C_{loss} is primarily dependent on the FEC and is defined in Eq. (12).

$$C_{loss} = k_{C\text{-}Rate}\, k_{DoC}\, FEC^{0.5} \tag{12}$$

In Eq. (12) the functions k_x describe the influences of the analyzed stress factors. These are the $C - Rate$ and the Depth of Cycle (DoC). The individual fitting functions are given in Eqs. (13) and (14). Since these functions are purely mathematical functions fitted through the capacity evolution of the respective test series, they are depicted without units in Naumann et al. (2020).

$$k_{C\text{-}Rate} = 0.0630\; C\text{-}Rate + 0.0971 \tag{13}$$

$$k_{DoC} = 4.0253\; (DoC - 0.5)^3 + 1.0923 \tag{14}$$

With regard to the nonlinearity of the degradation function and from the necessity of simulability in reasonable time, a one-dimensional optimization model is the only practical solution. In the linear optimization, the stress factors DoC as well as $C - Rate$ are assumed to be constant. The FEC are calculated with help of the cell capacity C_{Cell} and charge quantity throughput Q in Eq. (15).

$$FEC = \frac{Q}{2\, C_{Cell}} \tag{15}$$

Table 1 Characteristics of cell under review

Characteristic	Cell
Model	Sony US26650FTC1
Shape	Cylindrical
Electrodes	LiFePO4 (LFP); Graphite
Nominal capacity	2.85 Ah
Nominal voltage	3.65 V

The charge quantity throughput Q forms the continuous decision variable of the degradation function in the linear optimization. In Naumann et al. (2020), for the cyclic aging equation, the influence of the temperature is given via k_T. On our request to the authors of the study, k_T should be set to 1, since no temperature influence on the degradation between 25 °C and 40 °C in the test series could be determined. In addition, due to the impact of temperature on battery aging, EVs are commonly equipped with a Battery Thermal Management System (BTMS) ensuring that the battery pack remains within an optimal and safe temperature range.

General model structure

In eFlame, the aging model is implemented in a rolling optimization. A schematic visualization of the general model structure is shown in Fig. 3. The entire simulation period is divided into individual optimization steps with a predefined observation period. In each optimization step, the linear optimization problem is solved. Subsequently, the period is shifted by a fixed step size. The framework of the degradation model consists of two parts: Linear aging model and Nonlinear aging model.

The first part, a Linear aging model determines the opportunity costs from degradation for each optimization step. This part actively influences the charging strategy of the connected EVs in the optimization. The Linear aging model is implemented with both the pb-model and the wAh-model in order to enable a comparison of the two. To determine the opportunity costs from battery aging the capital expenditures for the battery Inv_{Bat} are applied as deprecation basis. From the literature review conducted in García-Miguel et al. (2022), this strategy proves to be the most common method. The expenditures are determined using battery pack prices from BloombergNEF's annual battery price surveys. Based on the 2021 release, the specific price of battery packs in EVs is $CP_{Bat} = 118$ \$/kWh (Veronika 2021). The EOL of the battery is set at a loss of 20 % of the initial capacity. This level was also set by IEEE standard 1188.1996. (Yao et al. 2021) The residual value of the battery after EoL_{Bat} is evaluated as 0 €. The second model part is a Nonlinear aging model. In this part

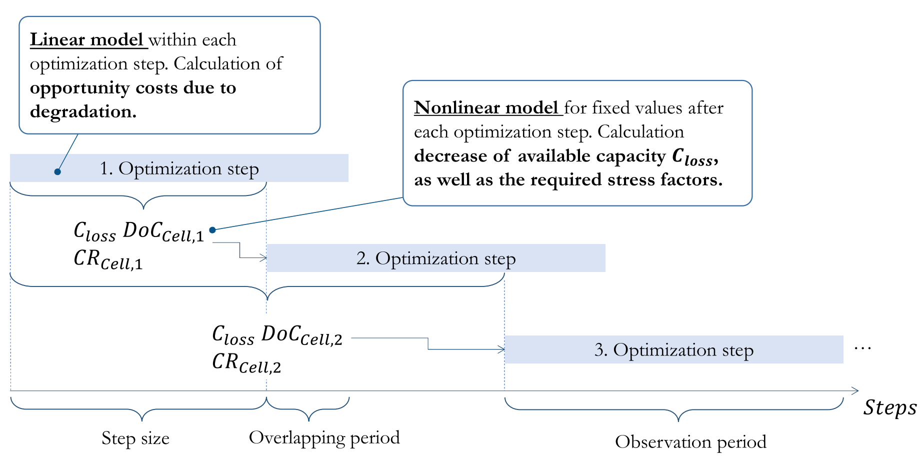

Fig. 3 Scheme of the degradation model in rolling optimization

of the model, the decrease in available capacity is always determined from the already fixed optimization results. In addition, the required constant stress factors for the linear aging model are generated. A continuous transfer of the results to the subsequent optimization step leads to a constant update of the Linear aging model. This results in an improvement of the accuracy. The aim with the continuous renewal of the constant stress factors is that the model itself generates the required stress factors as close to reality as possible from the prevailing conditions in the optimization.

Linear aging model

In this part of the model the choice whether the pb-model or the wAh-model should be used to calculate the degradation cost can be made during the scenario definition. Since the nonlinear course of degradation in Eq. (12) has to be implemented in a linear optimization, Fig. 4 demonstrates the principle of how this degradation is linearly approximated by the two models. The figure depicts a typical degradation course of C_{loss}, primarily caused by Q, from Eq. (12). Based on the maximum possible charge quantity throughput until the EOL $Q_{Cell-EoL,n,i}$ the wAh-model basically forms a line through the origin to determine the degradation caused by occurring Q. This means that the degradation costs are determined independently of the current SoH of the battery. The pb-model realizes a pieceswise linear approximation of the course of degradation beginning with the current SoH of the battery.

Performance based model

The calculation of the degradation costs C_{Deg} in € is based on the use of the battery and determined by the decrease of the available capacity C_{loss} from Eq. (12) in Cyclic aging model. For the pb-model the value is evaluated in every optimization step. Equation (16) forms the basic relationship for determining the cost.

$$C_{Deg} = \frac{Inv_{Bat}}{20\%} C_{loss}(Q, C\text{-}Rate, DoC) \tag{16}$$

In this way, for the implementation of the opportunity cost, the basic objective function from General model structure for every n-th optimization step in the rolling optimization is extended by the decision variable $C_{Deg,n,i}$. It represents the total degradation costs with N_{EV} EVs and is depicted in Eq. (17).

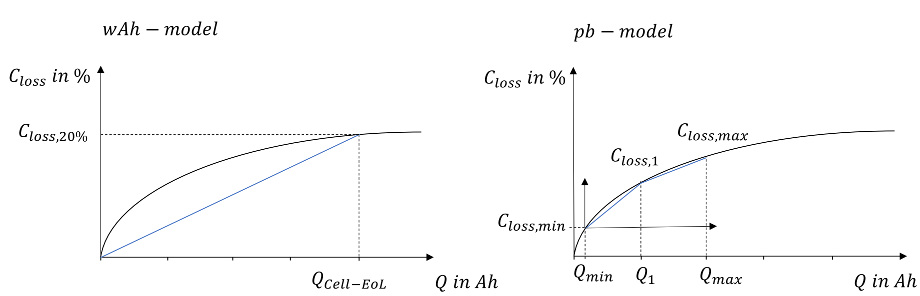

Fig. 4 Linear approximation of degradation in wAh-model and pb-model

$$max\Big(\sum_{t=1}^{N_{St}}(p_{to-grid,t}\, P_{to-grid,t}\ \Delta t - p_{from-grid,t}\, P_{from-grid,t}\ \Delta t) \\ -\sum_{i=1}^{N_{EV}} C_{Deg,n,i}\Big) \tag{17}$$

Regarding the rolling optimization, the observation period in the optimization step obtains the predefined length of $N_S t\ \Delta t$ hours. To use the degradation function C_{loss} in eFlame, it needs to be assumed that the aging of the battery in the EV is realized representatively based on the aging of the parameterized cell from the study. Thus, all cells installed in the battery age in the same way. Consequently, to determine the aging, the charge quantity throughput of a cell is calculated with help of the total energy throughput of the battery. Under this assumption, the individual cell is charged or discharged at the same $C - Rate$ as the battery. The current I within each time step Δt is assumed to be constant. The charge quantity throughput Q of a cell is thus calculated in Eq. (18).

$$Q = \ I\Delta t \tag{18}$$

By using the equations for the $C\text{-}Rate = \frac{I}{C_{Cell}}$ respectively $C\text{-}Rate = \frac{P_{EV-ch/dis}}{E_{EV-cap}}$, the total amount of charge quantity throughput for a single cell in a optimization step $Q_{Cell,n,i}$ can be calculated with Eq. (19).

$$Q_{Cell,n,i} = \ \frac{\sum_{t=1}^{N_{St}} (P_{EV-ch,t,i}\ \eta_{ch} + \frac{1}{\eta_{dis}}\ P_{EV-dis,t,i})}{E_{EV-cap,i}}\ C_{Cell}\ \Delta t \tag{19}$$

The parameters η_{ch} and η_{dis} represent charging and discharging efficiencies in Eq. (19). As already stated in General model structure, at the beginning of each optimization step, the current capacity loss as well as the values of the constant stress factors are transferred from the Nonlinear aging model to the Linear aging model. To account for these changing values, the degradation cost curve must be continuously adjusted. In this way, the concept of the virtual charge quantity throughput $Q_{virtual}$ is adopted from Naumann et al. (2020). The variable $Q_{virtual}$ represents the required charge quantity throughput to achieve the current incremental capacity loss $C_{rain\ loss,n,i}$ under the adjusted conditions for the i-th EV at the beginning of the n-th optimization step. Using Eq. (12) from Cyclic aging model, the virtual throughput $Q_{virtual,n,i}$ is obtained by Eq. (20).

$$Q_{virtual,n,i} = \ \frac{2\ C_{rain\ loss,n-1,i}}{\left(k_{C\text{-}Rate}(CR_{Cell,n-1,i})\ k_{DoC}(DoC_{Cell,n-1,i})\right)^2} \tag{20}$$

The variables $DoC_{Cell,n,i}$ and $CR_{Cell,n,i}$ represent constant stress factors from the Nonlinear aging model. In addition to the charge quantity throughput $Q_{Cell,n,i}$, the energy consumption from the driving $E_{EV-drive,t,i}$ and the resulting consumption of the public charging $E_{EV-pub,t,i}$ are also considered in the degradation cost function in Eqs. (21) and (22).

$$Q_{Cell-driv,n,i} = \left(\sum_{t=1}^{N_{St}} \frac{E_{EV-driv,t,i}}{E_{EV-cap,i}} \right) C_{Cell} \tag{21}$$

$$Q_{Cell-pub,n,i} = \left(\sum_{t=1}^{N_{St}} \frac{E_{EV-pub,t,i}}{E_{EV-cap,i}} \right) C_{Cell} \tag{22}$$

To gain the full degradation cost function in the n-th optimization step and the i-th EV Eq. (16) has to be adjusted to Eq. (23).

$$\begin{aligned} C_{Deg,n,i} = & \frac{Inv_{Bat}}{20\%} \Big[C_{loss} \big(Q_{Cell,n,i} + Q_{Cell-pub,n,i} + Q_{Cell-driv,n,i} \\ & + \ Q_{virtual,n,i}, CR_{Cell,n-1,i}, DoC_{Cell,n-1,i} \big) \\ & - \ C_{loss} \big(Q_{virtual,n,i}, CR_{Cell,n-1,i}, DoC_{Cell,n-1,i} \big) \Big] \end{aligned} \tag{23}$$

The difference between C_{loss} in Eq. (23) is formed because in the calculation of degradation costs only the current increase in aging is of interest. In the final step, the nonlinear degradation cost curve is piecewise linearly approximated by the convex combination method from D'Ambrosio et al. (2010).

Weighted Ah-throughput model

For the wAh-model the degradation costs are calculated with help of the cost factor $CF_{Deg,n,i}$ in €/kWh. The constant factor is determined at the beginning of every n-th optimization step in Eq. (24).

$$CF_{Deg,n,i} = \frac{Inv_{Bat}}{E_{Bat-EoL,n,i}} \tag{24}$$

$E_{Bat-Eol,n,i}$ is the maximum possible energy throughput until the EOL of the battery and is calculated for each optimization step with the adjusted constant stress factors from the Nonlinear aging model for each EV. Just as in the pb-model, the aging assessment of the battery is derived from the aging of the cell. The basis forms the maximum possible charge quantity throughput $Q_{Cell-EoL,n,i}$. Based on Eq. (12) on cell level in Cyclic aging model, $E_{Bat-Eol,n,i}$ is calculated with Eq. (25).

$$\begin{aligned} E_{Bat-Eol,n,i} = & E_{EV-cap,i} \frac{Q_{Cell-EoL,n,i}}{C_{Cell}} \\ = & 2E_{EV-cap,i} \left(\frac{20\%}{k_{C\text{-}Rate}(CR_{Cell,n-1,i}) k_{DoC}(DoC_{Cell,n-1,i})} \right)^2 \end{aligned} \tag{25}$$

To integrate $CF_{Deg,n,i}$ in the objective function the linear optimization is adjusted to Eq. (26).

$$max\left(\sum_{t=1}^{N_{St}} p_{to-grid,t}\ P_{to-grid,t}\ \Delta t - p_{from-grid,t}\ P_{from-grid,t}\ \Delta t \right. \\ \left. - \sum_{i=1}^{N_{EV}} \left(P_{EV-ch,t,i}\eta_{ch} + \frac{1}{\eta_{dis}}\ P_{EV-dis,t,i}\right)\ CF_{Deg,n,i}\ \Delta t\right) \tag{26}$$

Nonlinear aging model

In the rolling optimization, the nonlinear model is always called after the linear model is executed. As already mentioned, this part of the model determines the exact decrease of the available capacity and necessary constant stress factors for the subsequent optimization step. The basis for the calculation of the cyclic aging is the rainflow cycle-counting method. For the implementation, the Rainflow Counting Algorithm MATLAB-toolbox by Prof. Dr. Adam Niesłony in Niesłony (2009) is used. The counting method is used to decompose irregular load-time histories into the number of different types of cycles that occur (Standard Practices for Cycle Counting in Fatigue 2017). The algorithm applies the Three-Point Counting Technique in which cycle determination is always based on the evaluation of three successive extrema. (GopiReddy et al. 2015) This is also recommended by ASTM E1049-85. Originally developed for mechanical fatigue studies, the rainflow counting method is also used in the analysis of cyclic aging of batteries (cf. Xu et al. (2018); Chawla et al. (2010); Shi et al. (2018); Yao et al. (2021)). Applying the algorithm to the SoC history of the fixed optimization results, the obtained stress factors values for the DoC, $C - Rate$ and Q from each individual cycle can be used to calculate the incremental degradation of the battery. In this way the degradation function in Eq. (12) from Cyclic aging model is applied on each single cycle and in summation returns the current degradation of the battery. The average values of the occurring stress factors from the individual cycles are used to determine the constant stress factors $DoC_{Cell,n,i}$ and $CR_{Cell,n,i}$ for the Linear aging model.

Scenario definition

To analyze the implemented models and their influence on bidirectional charging strategies, a base scenario is defined. The driving profiles used for the scenario are taken from Schmidt-Achert et al. (2021). From the existing pool of driving profiles, three exemplary profiles were determined for closer analysis. The selection is based on the annual mileage and respectively one profile with low, medium and high annual mileage is selected. Table 2 shows the chosen profiles with their characteristics. The availability in % indicates how often the EV is plugged into the wallbox during the period under

Table 2 Annual mileage of examined driving profiles

Driving profile	Annual mileage [km]	Availability [%]
EV1	3429.49 (low)	89.4
EV2	15359.22 (medium)	64.5
EV3	43159.04 (high)	64.1

Table 3 Defined parameters baseline scenario

Category	Parameter	Value
Vehicle	$E_{EV-cap,i}$	**39 kWh** 57 kWh **123 kWh**
	$P_{EV-max\ ch,t,i}, P_{EV-max\ dis,t,i}$	**11 kW** 22 kW **50 kW**
	η_{ch}	92.6 %
	η_{dis}	92.1 %
User parameter	SoC_{EV-ini}	100 %
	$SoC_{EV-min\ con}$	30 %
	$SoC_{EV-min\ dep}$	70 %
	Plug-in rate	100 %
Market	$P_{to-grid,t}, P_{from-grid,t}$	intraday auction prices 2021 from EEX
	p_{levies}	18.2 cent/kWh
	$p_{levies-red}$	2 cent/kWh
	$P_{pubChar}$	50 cent/kWh
	EXR	1.18 €/$
Battery	CP_{Bat}	118 $/kWh
	$SoH_{Cell-ini}$	**90 %** 95 % **100 %**
	$DoC_{Cell-ini}$	0.31 %
	$CR_{Cell-ini}$	0.39 1/h
Resolution Optimization	Total optimization period	1 a
	Step size	10 d
	Observation horizon	20 d
	Time resolution	0.25 h

consideration. An overview of the defined input parameters is provided in Table 3. The values in blue text represent the values adjusted in the sensitivity analysis.

For the purchased electricity that is not fed back into the grid, the full levies *Plevies* are to be paid. This includes the value added tax (VAT) of 19 % for electricity. The variable $p_{levies-red}$ represents the reduced levies on discharged electricity at GCP (Zaccherini 2023). In the user parameters, the SoC values were set to allow sufficient flexibility for V2G during the connection time of the EVs. In order to consider bidirectional charging as comprehensively as possible, a plug-in rate of 100 % is selected when the EV is parked at home. This specifies that upon arrival, the EV is immediately plugged into the wallbox and available for bidirectional charging. Most charging stations for private homes have a maximum charging power of 11 or 22 kW (Hecht and Figgener 2020). In the base scenario, a maximum charging and discharging power of 22 kW is assumed. To analyze the influence of power limitation in the Sensitivity analysis the maximum charging power is reduced to 11 kW and increased to 50 kW (fast charging). The energy capacity $E_{EV-cap,i}$ of current EV batteries is mostly in the range of approximately 20–100 kWh. (Kampker, A. 2018) According to European sales figures of EVs for road transport in 2021, the 4 best-selling models are: Tesla Model 3, Renault ZOE, VW ID.3 and VW ID.4 (Henßler 2021). Based on the available energy capacities of these models, a mean value of 57 kWh was calculated and applied to $E_{EV-cap,i}$ (EV database 2017). For the Sensitivity analysis $E_{EV-cap,i}$ is adjusted to 39 kWh and 123 kWh. These values come from the *ev-database.org* and correspond on the one hand to the current highest usable energy capacity value in the database and on the other hand to the capacity of the Nissan Leaf (39 kWh), one of the most sold EVs (EV database 2017). For public charging, a price of 50 cent/kWh is assumed (Ambrosch 2022). Due to the non-linearity of aging in the pb-model an initial $SoH_{Cell-ini}$ of 95 % is selected. An explanation and closer analysis of the impact of $SoH_{Cell-ini}$ is given in Sensitivity analysis. The influence of this parameter is analyzed by varying $SoH_{Cell-ini}$ to 90 % and 100 %. To determine the initial stress factor value for the $DoC_{Cell-ini}$ in the rolling optimization, the base scenario was simulated with a larger pool of EVs from Schmidt-Achert et al. (2021) without aging influence. The average value forms $DoC_{Cell-ini}$. To reduce model complexity, the maximum $C - Rate$ is always used for $CR_{Cell-ini}$ in the first optimization step.

Results

Base scenario

To quantify the degradation, in each optimization step the incurred degradation costs are divided by the the total energy throughput. Thus, the degradation costs can be compared even if the observation horizons overlap. The calculated cost factor is given in cent/kWh. Figure 5 shows the calculated degradation costs from the base scenario in each optimization step for the two different models and three annual mileages. For the pb-model the average degradation cost over all three annual mileages is 0.45 cent/kWh. For the wAh-model the average degradation costs are 0.23 cent/kWh. The different levels of degradation costs are due to the different methods of approximating the non-linear course of the cell aging in Linear aging model. The cause for the higher degradation costs in the pb-model is that with a $SoH_{Cell-ini}$ of 95 % the slopes in the prevailing section

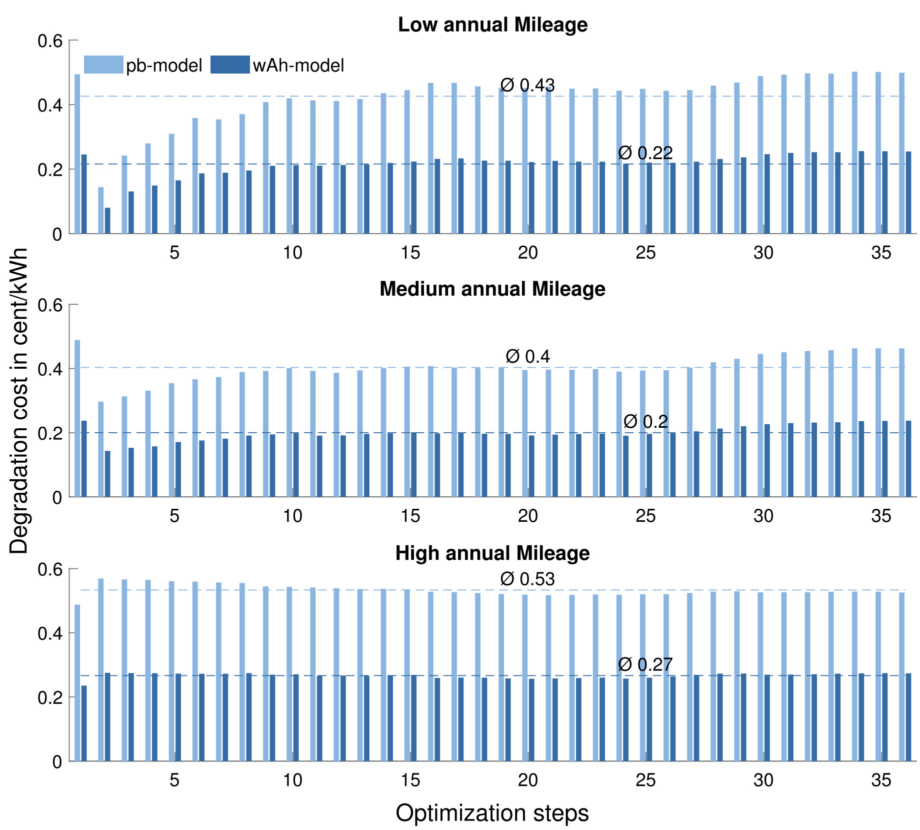

Fig. 5 Degradation costs of pb- and wAh-model

of the degradation curve are higher compared to the one in the wAh-model. (cf. Fig. 4) This is because the cell shows an increased degradation at the Beginning of Life (BoL) in the experimental series from Naumann et al. (2020). From a physical point of view, the piecewise approximation in the pb-model ensures a much more accurate approximation of the real aging of the cell compared to the wAh-model. In general, the accuracy of the model is of high importance, as otherwise important potentials are over- or underestimated due to, for example, oversimplifications. However, it is already apparent from this result that the current SoH has a significant impact on the economic analysis for bidirectional charging strategies. Regarding the deviation of the degradation costs between the optimization steps, the highest volatility occurs for the low annual mileage driving profile in both models. For the low annual mileage the relative standard deviation is 18.3 % and 17 % for the pb-model and wAh-model, respectively. Thus, for a more detailed understanding the following analysis focuses on the results obtained for the low annual mileage profile. For both models the cause of the volatile costs are the operating conditions of the battery, considering Q, $C - Rate$ and DoC. In general, it can be stated that the higher the DoCs respectively the $C - Rate$s, the higher the decrease in available capacity (Jenu et al. 2018; Omar et al. 2014). Indirectly, the relationship between the costs and the operation conditions can be derived from the amounts of energy throughput in the respective optimization steps. In the optimization, the energy throughput is composed of the driving consumption as well as the charging and discharging activities at the wallbox. The energy consumption from driving will not be considered in the further analysis of the low annual mileage profile results, since it only makes up 4.3 % of the total energy throughput in the pb-model and 4.0 % in the wAh-model for this driving profile. Additionally, for each optimization step the amount of energy charged and discharged needs to be the same. Therefore, Fig. 6 depicts the total discharged energy at the wallbox for the fixed results of each optimization step for the two models, as well as the simulation without aging, on the left axis. One optimization step represents the amount of discharged energy at the wallbox within 10 days.

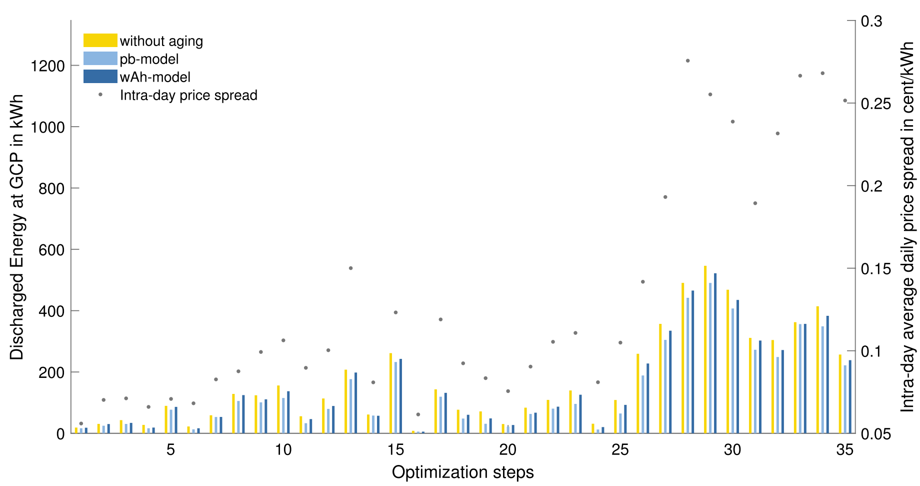

Fig. 6 Discharged energy at the wallbox for low annual mileage for each optimization step and daily average intraday price spreads

To explain these results, the average daily price spread of intraday auction trading within the observation horizon is depicted on the right axis in cent/kWh. The daily price spread refers to the differences between minimal and maximal intraday price for each day. This spread represent the revenue opportunities of bidirectional charging strategies, which means charging electricity at low spot prices and profitably discharging again at high prices. From Fig. 6 it can be seen that the discharge activities in each optimization step are mainly determined by the corresponding height of the price spreads. The correlation between the price spreads and the discharge activities is, on average, 94 %. At the beginning of the optimization, only a small amount of discharging activities take place. In the end, due to the higher spreads, significantly more energy is discharged. The results are lower degradation costs in the beginning, since the stress factors defining the slope of the degradation curve tend to be lower compared to the end. (cf. Fig. 5) The higher energy throughputs at the end of the optimization lead to higher DoCs. In the pb-model for the first quarter of the year the average DoC is 20.2 %, whereas in the last quarter the average DoC is 32.4 %. In the wAh-model the corresponding DoCs are 21.2 % respectively 31.8 %. Comparing the $C - Rate$s from the two quarters, small increases of 8.1 % to 0.36 1/h in the pb-model and 8.2 % to 0.35 1/h in the wAh-model are recorded. To give a general quantification of the influence of battery degradation on the charging strategy, the annual revenues generated by bidirectional charging of the EVs at the wallbox are considered. Figure 7 depicts the revenues in € of the three annual mileage profiles and compares the two models with the results from the simulation without aging. The results of the simulation without aging show on average a revenue stream of 678 € through bidirectional charging. This value is in a similar range to that in Kern et al. (2020). On average, the aging influence of the pb-model results in a revenue reduction of 3.0 % over the year. The wAh-model causes on average a decrease of 1.3 %. For both models the cyclic battery degradation only has minor influence on the revenues through arbitrage trading. However, regarding the amount of energy discharged at the wallbox, the pb-model leads on average to a decrease in discharged energy of 20 %. Similarly, the wAh-model reduces the amount of discharged energy by an average of 10.3 %. Thus, in the optimization model with aging,

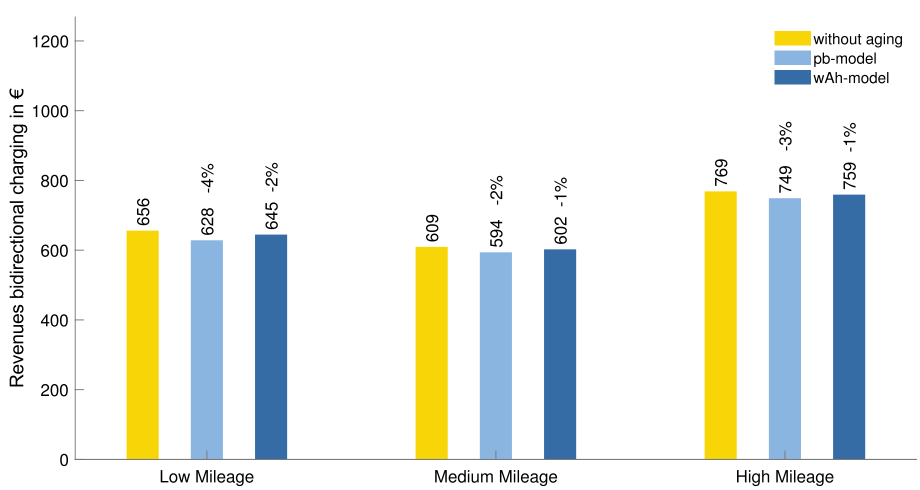

Fig. 7 Annual revenues from bidirectional charging in €/EV

Table 4 Average SoC of models in base scenario

Model	Low mileage	Medium mileage	High mileage
Without aging	73.8 %	73.3 %	65.4 %
pb-model	74.5 %	73.7 %	65.8 %
wAh-model	74.1 %	73.5 %	65.4 %

most of the revenue is generated by exploiting high price spreads. Consequently, smaller price spreads with less revenue potential are no longer exploited, leading to a decrease in discharge activities at the wallbox. Based on these results both models represent a valid option to include battery degradation in market optimization problems. From the literature, it can be seen that increased SoCs have a negative effect on the aging of LFP cells. (Omar et al. 2014) A limitation of the model results from the basic parameterization in Cyclic aging model, as the SoC does not influence the charging strategy in the optimization process. Table 4 displays the average SoCs from the base scenario.

Thus, from Table 4 it can be seen that throughout the simulation of the year heightened SoCs are prevailing.

Sensitivity analysis

To classify the results and to develop a more comprehensive understanding of the two models, a sensitivity analysis is carried out. Figure 8 shows the effect of the parameter variations described in the Scenario definition section on the occurring degradation cost in the optimization for each model. The degradation cost factor in cent/kWh is evaluated as average value regarding the three EVs for the full optimization period. For both charts, the horizontal axis represents the corresponding parameter variation starting from the base scenario. The two models show similar result developments, both for the variation of $E_{EV-cap,i}$ as well as $P_{EV-max\ ch,t,i}$ respectively $P_{EV-max\ dis,t,i}$.

When increasing $P_{EV-max\ ch,t,i}$ and $P_{EV-max\ dis,t,i}$ to 50 kW the pb-model displays a 56 % increase in degradation cost to 0.7 cent/kWh. In the wAh-model the degradation cost factor rises by 57 % to 0.36 cent/kWh. The reason for this increase lies in the

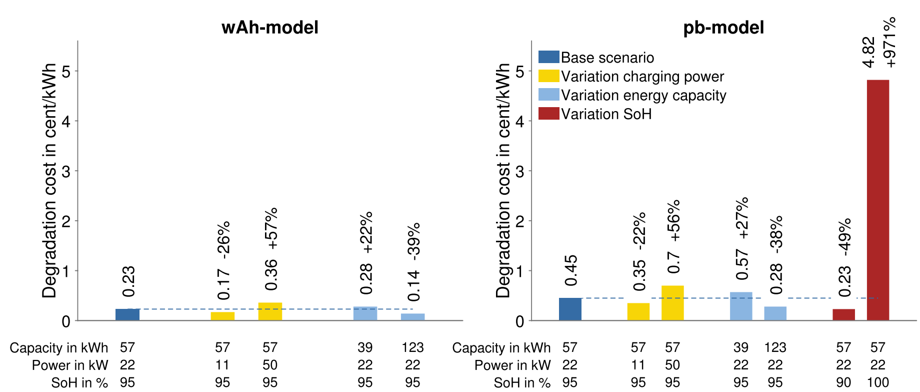

Fig. 8 Parameters influencing degradation cost in charging strategy

parametrization of the Cyclic aging model taking the $C - Rate$ as well as the DoC into account. Thus, an increase in the charging power inevitably enables higher $C - Rate$s, which lead to an increase in degradation cost. On average in the wAh-model, the $C - Rate$s rise by factor 2.1 to 0.72 1/h. An equal rise to 0.72 1/h occurs in the pb-model. For the DoCs there is an increase of 16.2 % and 14.3 % in the wAh-model respectively pb-model. Conversely, reducing $P_{EV-max\ ch,t,i}$ and $P_{EV-max\ dis,t,i}$ result in a lower degradation cost factor. Compared to the base scenario, applying a higher $E_{EV-cap,i}$ with equal $P_{EV-max\ ch,t,i}$ and $P_{EV-max\ dis,t,i}$ leads in both models to a decrease in $C - Rate$ by 51.6 %. On average the DoCs decrease by 34.7 %. Thus, despite the rising Inv_{Bat} in the optimization, the stress factor influence prevails and causes a lower degradation cost factor. Increasing the $E_{EV-cap,i}$ from 57 to 129 kWh in the wAh-model the degradation cost goes down by 39 % to 0.14 cent/kWh. For the pb-model, the same adjustment causes a decrease of 38 % to 0.28 cent/kWh. With the variation of $SoH_{Cell-ini}$, the influence of the more accurate approximation to the degradation curve within the pb-model becomes evident. Defining a $SoH_{Cell-ini}$ of 100 % results in a degradation cost factor of 4.82 cent/kWh. This means an increase of about factor 10 in the degradation cost. Whereas starting with a $SoH_{Cell-ini}$ of 90 % causes a decrease of 49 % to 0.23 cent/kWh. From this result, it can be seen that the current SoH in the pb-model has a significant impact on the economic analysis for bidirectional charging strategies. The cause of this development is the nonlinear aging of the battery. It becomes apparent that in the optimization the profitability of the arbitrage trading increases as the SoH of the battery decreases. This is because the high degradation at the BoL of the battery results in significantly higher degradation costs. In the applicability of degradation evaluation, the more accurate degradation model therefore proves to be suboptimal in the optimization. This leads to the conclusion that the wAh-model represents a better strategy to include battery degradation in market optimization problems.

Conclusion

Referring to the first research question of what aging models have been published, there are two particularly suitable methods that are appropriate for assessing battery aging in market optimization models: wAh-models with a fixed degradation cost factor, and pb-models that link the degradation to quantifiable indicators like capacity reduction. By elaborating on the second research question, the two models are analyzed and implemented into an existing optimization model. Both degradation models directly influence the charging strategy in the optimization by considering cyclic aging in the form of the percentage decrease in cell capacity. In addition, both models are an one-dimensional optimization problem with the decision variable Q and are developed in a rolling optimization. To increase accuracy, a nonlinear model component outside of the optimization ensures a continuous update of the two linear degradation models. Assessing the last research question, addressing the impact of battery aging on bidirectional charging strategies, the results show that the pb-model decreases the revenue potential on average by 3 % and the wAh-model by 1.3 %. The pb-model reveals that the SoH of the battery has a strong impact on the degradation cost of the battery. Thus, for the pb-model the course of the battery aging results in excessive degradation costs at the BoL. A more ideal strategy in the optimization proves to be the wAh-model, by calculating a constant cost factor independent of the current SoH. Therefore, even though from a physical perspective the pb-model is closer to the real cyclic aging of the battery, the wAh-model obtaining a more economical view represents the better option for cost optimization problems.

Abbreviations

ANN-model	Artificial Neural Network models
BoL	Beginning of Life
BTMS	Battery Thermal Management System
DoC	Depth of Cycle
DoD	Depth of Discharge
eFlame	electric Flexibility Assessment Modelling Environment
EOL	End of life
EV	electric vehicles
FEC	full equivalent cycles
GCP	grid connection point
LFP	LiFePO4
pb-model	performance based model
SoC	State of Charge
SoH	State of Health
V2G	vehicle-to-grid
VAT	value added tax
wAh-model	weighted Ah-throughput model

Glossary

$CF_{Deg,n,i}$	Degradation cost factor in €/kWh
CP_{Bat}	Weighted battery pack price €/kWh
$CR_{Cell,n,i}$	Mean C-rate as constant stress factor for n-th optimization step in linear model in 1/h for the i-th EV
$C-Rate$	Measure of the rate at which a battery is discharged or charged relative to its maximum capacity in 1/h
C_{Cell}	Nominal capacity of the cell in kWh
$CF_{Deg,n,i}$	Degradation cost battery in a optimization step in €for the i-th EV
C_{Deg}	Degradation cost battery in €
C_{loss}	Decrease in available capacity from cyclic aging of the cell in %
$C_{rain\ loss,n,i}$	Total loss of available capacity from non-linear model in n-th optimization step in %
$Con_{EV,t,i}$	Binary variable to indicate when i-th EV is connected (1) to the wallbox
$DoC_{Cell,n,i}$	Mean DoC as constant stress factor for n-th optimization step in linear model in % for the i-th EV
EXR	Average anual exchange rate €/$
$E_{Bat-EoL,n,i}$	Maximum possible energy throughput until the EoL of the battery in kWh
$E_{EV-buffer,t,i}$	Deviating amount of energy EV in time step t to $So_{CEV-min\ con}$ or $So_{CEV-min\ dep}$ in kWh
$E_{EV-cap,i}$	Energy capacity of the i-th EV in kWh
$E_{EV-driv,t,i}$	Energy consumption of the i-th EV while driving in time step t in kWh
$E_{EV-pub,t,i}$	Public charging of the i-th EV while driving in time step t in kWh
$E_{EV-stored,t,i}$	Energy capacity of EV in time step t in kWh
EoL_{Bat}	End of life of the battery in terms of the remaining available capacity of the battery in %
I	Current in A
Inv_{Bat}	Investment costs battery in €
N_{EV}	Number of EVs simulated in the optimization model
N_{St}	Number of time steps in the observation period from the optimization step
$P_{EV-ch,t,i}$	Occurring charging power of the i-th EV in time step t in kW
$P_{EV-dis,t,i}$	Occurring discharging power of the i-th EV in time step t in kW
$P_{EV-max\ ch,t,i}$	Maximum charging power from wallbox in time step t in kW
$P_{EV-max\ dis,t,i}$	Maximum discharging power from wallbox in time step t in kW
$P_{GCP-max,t}$	Maximum grid connection power in time step t in kW
$P_{from-grid,t}$	Power taken from the grid to the connected components in time step t in kW
$P_{to-grid,t}$	Fed in power at grid connection point in time step t in kW
Q	Charge quantity throughput in Ah
$Q_{Cell,n,i}$	Charge quantity throughput through cell in n-th optimization step in Ah for the respective EV

$Q_{Cell-EoL,n,i}$	Maximum possible charge quantity throughput in Ah until the EoL of the cell in Ah for the i-th EV in the n-th optimization step
$Q_{Cell-EoL,n,i}$	Maximum possible charge quantity throughput until the EoL of the cell in Ah
$Q_{virtual,n,i}$	Virtual charge charge quantity throughput to achieve the current C_{loss} under changed conditions in n-th optimization step in Ah for the i-th EV
$Q_{virtual}$	Virtual charge charge quantity throughput to achieve the current C_{loss} under changed conditions in Ah
$SoC_{EV,t,i}$	SoC of the i-th EV in time step t in %
$SoC_{EV.ini}$	Initial SoC of EV in %
SoC_{EV-min}	Con Minimum SoC when EV is plugged into GCP in %
$SoC_{EV-min\ dep}$	Minimum SoC when the EV departs in %
$SoH_{Cell-ini}$	Initial SoH of the cell in %
η_{ch}	Efficiency of charging the EV in %
η_{dis}	Efficiency of discharging the EV in %
i	Index for specifying the EV $(i \in \mathbb{N})$
k_x	Fitting function to wheight the cyclic degradation function with stress factors
n	Index for specifying the optimization step $(i \in \mathbb{N})$
$p_{from-grid,t}$	Corresponding price in time step t (costs) in €/kWh
$p_{levies-red}$	Reduced levies and charges on electricity fed back into the grid and the losses incurred during the (dis-)charging of this energy in €/kWh
p_{levies}	Levies on purchased electricity in €/kWh
$p_{pubChar}$	Cost for public charging in €/kWh
$p_{to-grid,t}$	Corresponding price in time step t (revenues) in €/kWh
t	Index for specifying the time step in optimization $(t \in \mathbb{N})$
$CR_{Cell.ini}$	Initial C-rate as stress factor in the linear model for the first optimization step in 1/h
$DoC_{Cell.ini}$	Initial DoC as stress factor in the linear model for the first optimization step in %

Author contributions
VP and FB conceived the idea for the study. VP conducted the literature research and designed the model. FB verified the analytical methods and defined the simulation scenarios. Under the supervision of FB the simulation and evaluation was carried out by VP. Both authors discussed the results and contributed to the final manuscript.

About this supplement
This article has been published as part of Energy Informatics Volume 6 Supplement 1, 2023: Proceedings of the 12th DACH+ Conference on Energy Informatics 2023. The full contents of the supplement are available online at https://energyinformatics.springeropen.com/articles/supplements/volume-6-supplement-1.

Funding
This research was conducted as part of the activities of the FfE in the project Trade-EVs II funded by the Federal Ministry of Economics and Climate Action (BMWK) (funding code: 01MV20006E).

Availability of data and materials
No further data is attached to this paper.

Declarations

Competing interests
The authors declare that they have no competing interests.

Published: 19 October 2023

References

Ambrosch T (2022) E-Auto Laden Kosten: Das Zahlst du Zuhause und Unterwegs. https://emobia.de/e-auto-laden-kosten/. Accessed 25 April 23

Bolay LJ, Schmitt T, Hein S, Mendoza-Hernandez OS, Hosono E, Asakura D, Kinoshita K, Matsuda H, Umeda M, Sone Y, Latz A, Horstmann B (2022) Microstructure-resolved degradation simulation of lithium-ion batteries in space applications. J Power Sour Adv 14:100083

Brinkel NBG, Schram WL, Al Skaif TA, Lampropoulos I, van Sark WGJHM (2020) Should we reinforce the grid? cost and emission optimization of electric vehicle charging under different transformer limits. Appl Energy 276:115285

Bantle C, Metz J (2019) Bundesverband der Energie- und Wasserwirtschaft e.V.: Meinungsbild E-Mobilität. https://www.bdew.de/media/documents/Awh_20190527_Fakten-und-Argumente-Meinungsbild-E-Mobilitaet.pdf. Accessed 10 April 23

Chawla M, Naik R, Burra R, Wiegman H (2010) Utility energy storage life degradation estimation method. In: 2010 IEEE Conference on Innovative Technologies for an Efficient and Reliable Electricity Supply. IEEE, Waltham, MA, USA

D'Ambrosio C, Lodi A, Martello S (2010) Piecewise linear approximation of functions of two variables in MILP models. Oper Res Lett 38(1):39–46
Ekström H, Lindbergh G (2015) A model for predicting capacity fade due to sei formation in a commercial graphite/lifepo4 cell. J Electrochem Soc 162(6):1003–1007
Erdinc O, Vural B, Uzunoglu M (2009) A dynamic lithium-ion battery model considering the effects of temperature and capacity fading
EV Database (2017). https://ev-database.org/cheatsheet/useable-battery-capacity-electric-car. Accessed 28 Mar 2023
Farzin H, Fotuhi-Firuzabad M, Moeini-Aghtaie M (2016) A practical scheme to involve degradation cost of lithium-ion batteries in vehicle-to-grid applications. IEEE Trans Sustain Energy 7(4):1730–1738
García-Miguel PLC, Alonso-Martínez J, Gómez SA, Plaza MG, Asensio AP (2022) A review on the degradation implementation for the operation of battery energy storage systems. Batteries 8(9):110
Geringer B, Tober W (2012) Batterieelektrische Fahrzeuge in der Praxis: Kosten, Reichweite, Umwelt, Komfort (2. erweiterte und korrigierte Auflage). Institut für Fahrzeugantriebe und Automobiltechnik, Technische Universität Wien, Österreichische Verein für Kraftfahrzeugtechnik (ÖVK); A-1010 Wien, Elisabethstraße 26, Berichts-Nr. B12020, 2012; 79 S
Gopi Reddy L. R., Tolbert L. M., Ozpineci B., Pinto J. O. P. (2015) Rainflow algorithm-based lifetime estimation of power semiconductors in utility applications. IEEE Trans Ind Appl 51(4):3368–3375
Hecht C, Figgener J (2022) Elektroauto-Boom 2020: Neuzulassungen Mit 9 Gigawattstunden Batteriekapazität. https://www.pv-magazine.de/2021/03/12/elektroauto-boom-2020-neuzulassungen-mit-9-gigawattstunden-batteriekapazitaet/. Accessed 27 April 2023
Henßler S (2022) Das Waren die Zehn Meistverkauften E-Autos 2021 in Europa. https://www.elektroauto-news.net/2022/zehn-meistverkauften-e-autos-2022-europa. Accessed 10 Mar 2023
Hinterstocker M, Ostermann A, Müller M, Dossow P et al. (2019) Bidirectional charging management-field trial and measurement concept for assessment of novel charging strategies. https://www.ffe.de/en/publications/bidirectional-charging-management-field-trial-and-measurement-concept-for-assessment-of-novel-charging-strategies/. Accessed 14 April 23
Huss A, Maas H, Hass H (2013) JEC WELL-TO-WHEELS ANALYSIS. European Commission. Joint Research Centre, Ispra, Italy
Jenu S, Tuurala S, Manninen A et al. (2018) Simplified State of Health Diagnostics Tool. https://ec.europa.eu/research/participants/documents/downloadPublic?documentIds=080166e5c014c65e&appId=PPGMS. Accessed 24 Feb 2023
Johnson VH (2002) Battery performance models in ADVISOR. J Power Sources 110(2):321–329
Kampker A (2018) Elektromobilität: Grundlagen Einer Zukunftstechnologie. Deutschland, Springer, Berlin, p 344
Kern T, Bukari B (2021) Peak shaving - a cost-benefit analysis for different industries. In: 12. Internationale Energiewirtschaftstagung an der TU Wien. TU Wien, Wien
Kern T, Dossow P, von Roon S (2020) Integrating bidirectionally chargeable electric vehicles into the electricity markets. Energies 13(21):5812
Kern T, Dossow P, Morlock E (2022) Revenue opportunities by integrating combined vehicle-to-home and vehicle-to-grid applications in smart homes. Appl Energy 307:118187
Kern T, Biedenbach F, Schmidt-Achert T (2023) eFlame - Electric flexibility assessment modeling environment. https://www.ffe.de/tools/eflame-electric-flexibility-assessment-modeling-environment/. Accessed 03 Mar 2023
Liaw BY, Jungst RG, Nagasubramanian G, Case HL, Doughty DH (2005) Modeling capacity fade in lithium-ion cells. J Power Sources 140(1):157–161
Naumann M, Spingler FB, Jossen A (2020) Analysis and modeling of cycle aging of a commercial LiFePO4/graphite cell. J Power Sources 451:227666
Niesłony A (2009) Determination of fragments of multiaxial service loading strongly influencing the fatigue of machine components. Mech Syst Signal Process 23(8):2712–2721
Omar N, Monem MA, Firouz Y, Salminen J, Smekens J, Hegazy O, Gaulous H, Mulder G, den Bossche PV, Coosemans T, Mierlo JV (2014) Lithium iron phosphate based battery assessment of the aging parameters and development of cycle life model. Appl Energy 113:1575–1585
Pellinger C., Schmid T. (2012) Merit Order der Energiespeicherung Im Jahr 2030 (MOS 2030). https://www.ffe.de/projekte/mos/. Accessed 08 Mar 2023)
Prada E, Domenico DD, Creff Y, Bernard J, Sauvant-Moynot V, Huet F (2013) A simplified electrochemical and thermal aging model of lifepo4-graphite li-ion batteries: Power and capacity fade simulations. J Electrochem Soc 160(4):616–628
Samweber F, Köppl S et al. (2017) Projekt MONA 2030: Abschlussbericht Einsatzreihenfolgen Veröffentlicht. https://www.ffe.de/veroeffentlichungen/projekt-mona-2030-abschlussbericht-einsatzreihenfolgen-veroeffentlicht/. Accessed 04 Mar 2023
Schimpe M, Truong CN, Naumann M, Jossen A, Hesse HC, Reniers JM, Howey DA (2018) Marginal costs of battery system operation in energy arbitrage based on energy losses and cell degradation. In: 2018 IEEE International Conference on Environment and Electrical Engineering and 2018 IEEE Industrial and Commercial Power Systems Europe. IEEE, Palermo, Italy
Schmalstieg J, Käbitz S, Ecker M, Sauer DU (2014) A holistic aging model for li(NiMnCo)o2 based 18650 lithium-ion batteries. J Power Sources 257:325–334
Schmidt-Achert T, Bogensperger A, Fattler S, Ostermann A (2021) Using clustering algorithms to identify representative EV mobility profiles for complex energy system models. In: 5th E-Mobility Power System Integration Symposium (EMOB 2021). Institution of Engineering and Technology, Hybrid Conference, Germany
Seydenschwanz M, Majewski K, Gottschalk C, Fink R (2019) Linear approximation of cyclic battery aging costs for MILP-based power dispatch optimization. In: 2019 IEEE PES Innovative Smart Grid Technologies Europe (ISGT-Europe). IEEE, Bucharest, Romania
Shen WX, Chau KT, Chan CC, Lo EWC (2005) Neural network-based residual capacity indicator for nickel-metal hydride batteries in electric vehicles. IEEE Trans Veh Technol 54(5):1705–1712
Shi Y, Xu B, Tan Y, Zhang B (2018) A convex cycle-based degradation model for battery energy storage planning and operation. In: 2018 Annual American Control Conference (ACC). IEEE, Milwaukee, WI, USA

Soleimani A, Vahidinasab V, Aghaei J (2021) Enabling vehicle-to-grid and grid-to-vehicle transactions via a robust home energy management system by considering battery aging. In: 2021 International Conference on Smart Energy Systems and Technologies (SEST). IEEE, Vaasa, Finland

Standard Practices for Cycle Counting in Fatigue Analysis (2017). https://www.astm.org/e1049-85r17.html. Accessed 17 Mar 2023

Swierczynski M, Stroe D-I, Stan A-I, Teodorescu R, Kaer SK (2015) Lifetime estimation of the nanophosphate lifepo4/c battery chemistry used in fully elec-tric vehicles. IEEE Trans Ind Appl 51(4):3453–3461

Veronika H (2021) Battery pack prices fall to an average of \$132/kWh, but rising commodity prices start to bite. https://about.bnef.com/blog/battery-pack-prices-fall-to-an-average-of-132-kwh-but-rising-commodity-prices-start-to-bite/. Accessed 19 Mar 2023

Wang J, Liu P, Hicks-Garner J, Sherman E, Soukiazian S, Verbrugge M, Tataria H, Musser J, Finamore P (2011) Cycle-life model for graphite-LiFePO4 cells. J Power Sources 196(8):3942–3948

Xu B, Oudalov A, Ulbig A, Andersson G, Kirschen DS (2018) Modeling of lithium-ion battery degradation for cell life assessment. IEEE Trans Smart Grid 9(2):1131–1140

Yao L, Xu S, Tang A, Zhou F, Hou J, Xiao Y, Fu Z (2021) A review of lithium-ion battery state of health estimation and prediction methods. World Electr Veh J 12(3):113

Zaccherini C (2023) BDEW-Strompreisanalyse Jahresbeginn 3023. https://www.bdew.de/service/daten-und-grafiken/bdew-strompreisanalyse/. Accessed 11 Mar 2023

Zhou C, Qian K, Allan M, Zhou W (2011) Modeling of the cost of ev battery wear due to v2g application in power systems. IEEE Trans Energy Convers 26(4):1041–1050

Zhou K, Cheng L, Lu X, Wen L (2020) Scheduling model of electric vehicles charging considering inconvenience and dynamic electricity prices. Appl Energy 276:115455

Publisher's Note

Springer Nature remains neutral with regard to jurisdictional claims in published maps and institutional affiliations.